Received: 9 February 2023 | Revised: 14 May 2023 | Accepted: 16 May 2023

DOI: 10.1002/mma.9458

RESEARCH ARTICLE

WILEY

High-order schemes and their error analysis for generalized variable coefficients fractional reaction–diffusion equations

Anshima Singh[1] | **Sunil Kumar**[1] | **Jesus Vigo-Aguiar**[2]

[1]Department of Mathematical Sciences, Indian Institute of Technology (BHU) Varanasi, Varanasi, Uttar Pradesh, India

[2]Department of Applied Mathematics, University of Salamanca, Salamanca, Spain

Correspondence
Anshima Singh, Department of Mathematical Sciences, Indian Institute of Technology (BHU) Varanasi, Varanasi, Uttar Pradesh, India.
Email: anshima.singh.rs.mat18@itbhu.ac.in

Communicated by: C. Cuevas

In this manuscript, we develop and analyze two high-order schemes, $\text{CFD}_{g-\sigma}$ and $\text{PQS}_{g-\sigma}$, for generalized variable coefficients fractional reaction–diffusion equations. The generalized fractional derivative is characterized by a weight function and a scale function. We approximate it using generalized Alikhanov formula ($gL2-1_\sigma$) of order $(3-\mu)$, where μ $(0 < \mu < 1)$ denotes the order of the generalized fractional derivative. Moreover, for spatial discretization, we use a compact operator in $\text{CFD}_{g-\sigma}$ scheme and parametric quintic splines in $\text{PQS}_{g-\sigma}$ scheme. The stability and convergence analysis of both schemes are demonstrated thoroughly using the discrete energy method in the L_2-norm. It is shown that the convergence orders of the $\text{CFD}_{g-\sigma}$ and $\text{PQS}_{g-\sigma}$ schemes are $O(\Delta t^{3-\mu}, \widetilde{\Delta} t^2, h^4)$ and $O(\Delta t^{3-\mu}, \widetilde{\Delta} t^2, h^{4.5})$, respectively, where Δt and $\widetilde{\Delta} t$ represent the mesh spacing in the time direction and h is the mesh spacing in the space direction. In addition, numerical results are obtained for three test problems to validate the theory and demonstrate the efficiency and superiority of the proposed schemes.

KEYWORDS

$gL2-1_\sigma$ formula, generalized fractional derivative, high order, parametric quintic spline, reaction–diffusion equation

MSC CLASSIFICATION

65M06, 65M12, 65M70, 35R11

1 | INTRODUCTION

During the last few decades, fractional differential equations have gained much attention, as the hereditary and memory properties of fractional derivatives have improved the accuracy of models. These equations have found applications in several areas, including viscoelasticity, control theory, signal processing, material science, finance, acoustics, electromagnetics, electrical networks, material science, physics, biological systems, nuclear reactor dynamics, fluid mechanics, and optics [1–13]. Further, the study of reaction–diffusion equations has always been a hot topic for researchers because of their various real-world applications. These problems are important for environmental science in examining pollution from industrial waste material (or manufacturing sources) entering the atmosphere [14]. Through such problems, the reaction and diffusion processes of components in porous catalysts have long been researched in [15, 16]. Moreover, there are a plenty of real-world problems, such as logistic population growth [17], chemical reactions [18], nuclear reactor theory, and branching Brownian motion processes, that can be modeled using the reaction–diffusion equations.

In literature, there are a number of definitions of fractional derivatives, namely, Riemann–Liouville derivative, Grunwald–Letnikov derivative, Caputo derivative, Riesz derivative, and regularized Ψ-Hilfer fractional derivative [1, 2, 19]. These definitions have been featured prominently in the field of fractional calculus and have been used to model many physical phenomena. Due to the application of different procedures, the generalization of fractional integral (or derivative) from integer integral (or derivative) may not be unique. To unify the various procedures, Agrawal [20] has given a new generalized fractional derivative (GFD), which unifies some famous fractional derivatives, like Riemann–Liouville, Caputo, modified Erdélyi–Kober, and Hadamard. The GFD involves a weight function $\omega(t)$ and a scale function $z(t)$. The scale function can contract or stretch the domain, whereas the weight function can weigh the solution at different time levels. Moreover, the choice of different scale and weight functions provide famous fractional derivatives. Indeed, many other types of fractional derivatives can be obtained by varying the scale and weight functions, which may either be entirely new or already known. The problems involving GFDs are very difficult to solve analytically, except for a small class of problems [21, 22]. Consequently, it is important to solve generalized fractional differential equations numerically. Some pioneering works [22–27] have contributed to numerically solving some generalized fractional problems.

In this work, we consider the following generalized fractional reaction–diffusion problem with variable coefficients, which is more general than that in [22, 23, 25]:

$$ {}_0^C D^{\mu}_{t:[z(t),\omega(t)]} v(x,t) + q(t)v(x,t) = p(t)\frac{\partial^2 v(x,t)}{\partial x^2} + \mathscr{F}(x,t), (x,t) \in (0,b)\times(0,T), \tag{1} $$

with initial condition

$$ v(x,0) = g_0(x), x \in [0,b], \tag{2} $$

and boundary conditions

$$ \begin{cases} v(0,t) = \hat{\phi}_1(t),\ t \in (0,T], \\ v(b,t) = \hat{\phi}_2(t),\ t \in (0,T], \end{cases} \tag{3} $$

where $0 < \mu < 1$, $q \geq 0$, $p > p_0 \geq 0$, g_0, $\hat{\phi}_1$, $\hat{\phi}_2$, and $\mathscr{F}$ are known sufficiently smooth functions. Moreover, ${}_0^C D^{\mu}_{t:[z(t),\omega(t)]}$ denotes the generalized fractional differential operator defined in [20] as

$$ {}_0^C D^{\mu}_{t:[z(t),\omega(t)]} v(x,t) = \frac{[\omega(t)]^{-1}}{\Gamma(1-\mu)} \int_0^t (z(t)-z(s))^{-\mu} \frac{\partial\,(\omega(s)v(x,s))}{\partial s} ds. \tag{4} $$

To smoothen the development and analysis of the methods, we write an equivalent form of (1)–(3) with the unity weight function $\omega(t)$ and the same scale function $z(t)$ by setting $u(x,t) = \omega(t)v(x,t)$:

$$ {}_0^C D^{\mu}_{t:[z(t),1]} u(x,t) + q(t)u(x,t) = p(t)\frac{\partial^2 u(x,t)}{\partial x^2} + F(x,t), (x,t) \in (0,b)\times(0,T), \tag{5} $$

with initial condition

$$ u(x,0) = g(x), x \in [0,b], \tag{6} $$

and boundary conditions

$$ \begin{cases} u(0,t) = \phi_1(t),\ t \in (0,T], \\ u(b,t) = \phi_2(t),\ t \in (0,T], \end{cases} \tag{7} $$

where $g(x) = \omega(0)g_0(x)$, $\phi_1(t) = \omega(t)\hat{\phi}_1(t)$, $\phi_2(t) = \omega(t)\hat{\phi}_2(t)$, and $F(x,t) = \omega(t)\mathscr{F}(x,t)$. Once the numerical solution of problem (5)–(7) is obtained, one can easily compute the numerical solution of problem (1)–(3) by $u(x,t) = \omega(t)v(x,t)$.

There are many ways to construct high-order numerical methods in the literature. Among them, the use of compact difference operators is well known. High-order compact scheme was first used in [28] to solve the scalar wave equation. After that, a number of works have been done to solve various classes of differential equations using compact scheme [29–35]. Moreover, there are a few more techniques to approximate the space variable, such as hybrid schemes [36–39], spline collocation methods [40–42], and non-polynomial splines. Khan et al. [43] first introduced the non-polynomial spline

method to approximate integer-order differential equations. Subsequently, the fractional subdiffusion problem [44] and fractional Burger's equation [45] have been successfully solved using a parametric cubic spline, which is a non-polynomial spline. The authors of [43–45] showed that non-polynomial spline methods yield better numerical results than some previously existing works, but they did not fully demonstrate the theoretical analysis (convergence and stability) of such methods. Further, in [46], the authors established and analyzed an efficient numerical method for fractional subdiffusion equations. They used the well-known L-1 formula to discretize the Caputo fractional derivative and the parametric quintic spline for spatial discretization.

Most of the existing works (such as [22, 23, 25] and the references therein) for the present model problem consider the problem without the reaction term and with a constant $p(t)$. So, it is required to consider a more general problem with variable coefficients. Further, they discretized the space variable using a second-order central difference scheme. So, the resulting fully discrete schemes are low-order accurate. Observe that high-order numerical methods have great significance because they result in more accurate approximations. So, it is important to develop high-order numerical methods for the present problem. Hence, this article aims to fill these gaps in the literature.

We develop and analyze two high-order schemes $\text{CFD}_{g-\sigma}$ and $\text{PQS}_{g-\sigma}$ for numerically solving problem (5)–(7). To this end, we consider the $(3-\mu)$th order generalized Alikhanov formula ($gL2-1\sigma$) to approximate the generalized time-fractional derivative, together with two high-order schemes for spatial discretization. In the $\text{CFD}_{g-\sigma}$ scheme, we consider a fourth-order compact difference operator to discretize the spatial derivative, while in the $\text{PQS}_{g-\sigma}$ scheme, we consider a parametric quintic spline scheme to discretize the spatial derivative. Furthermore, for the developed schemes, we thoroughly discuss the stability and convergence analysis and show that the theoretical bounds for the $\text{CFD}_{g-\sigma}$ and $\text{PQS}_{g-\sigma}$ schemes are $O(\Delta t^{3-\mu}, \widetilde{\Delta} t^2, h^4)$ and $O(\Delta t^{3-\mu}, \widetilde{\Delta} t^2, h^{4.5})$, respectively, where Δt and $\widetilde{\Delta} t$ represent the mesh spacing in the time direction and h is the mesh spacing in the space direction. Also, to show the accuracy and efficiency of our schemes, we perform numerical experiments on three well-known test problems and compare the results with existing ones.

Organization of the paper: In Section 2, we develop two high-order fully discrete numerical schemes for solving the generalized fractional reaction–diffusion problem. Stability and convergence of both the schemes in L_2- norm have been established separately in Section 3. Further, the numerical results of the developed numerical schemes are discussed in Section 4 with the help of three test problems. Finally, Section 5 concludes the paper.

2 | NUMERICAL SCHEMES

In this section, first, we will provide the approximation of the GFD. Then, we will obtain two high-order fully discrete numerical schemes that approximate problem (5)–(7).

2.1 | Discretization of GFD

Throughout this work, we suppose that z (the scale function) is a strictly increasing function. Suppose $\mathcal{Z} : t \to z(t)$ is a mapping from $[0, T]$ to $[z(0), z(T)]$. Suppose N_t is a positive integer. We divide the interval $[0, T]$ into N_t subintervals with nonuniform partition $\Omega_t : 0 = t_0 < t_1 < \cdots < t_{N_t} = T$. Now denote $z(t_j) = z_j$ and consider $z_j = z_0 + j\Delta t$ and $t_j = \mathcal{Z}^{-1}(z_0 + j\Delta t)$, where $\Delta t = \frac{z(T)-z(0)}{N_t} = z(t_{j+1}) - z(t_j)$, $0 \le j \le N_t - 1$. Furthermore, let $\widetilde{\Delta} t = \max_{0\le j\le N_t-1}(t_{j+1} - t_j)$.

Now, let $\sigma = 1 - \frac{\mu}{2}$. Here, it is obvious that $z(t_{j+\sigma}) = z_{j+\sigma} = z_0 + (j+\sigma)\Delta t$ and $t_{j+\sigma} = \mathcal{Z}^{-1}(z_0 + (j+\sigma)\Delta t)$ for $0 \le j \le N_t - 1$. Then, generalized Alikhanov formula ($gL2-1_\sigma$) for the GFD of function $G(\mathcal{Z}^{-1}(z)) \in C^3[z(0), z(T)]$ at $t_{j+\sigma}$ is given by [25]

$$ {}_0^C D^{\mu}_{t:[z(t),1]} G(t_{j+\sigma}) = \nu \left[w_0 G(t_{j+1}) - \sum_{k=1}^{j} (w_{j-k} - w_{j-k+1}) G(t_k) - w_j G(t_0) \right] + O(\Delta t^{3-\mu}), \tag{8} $$

where $\nu = \frac{\Delta t^{-\mu}}{\Gamma(2-\mu)}$ and the coefficients w_k's are given as $w_0 = a_0$, if $j = 0$, and for $j \ge 1$

$$ w_k = \begin{cases} a_0 + b_1, & k = 0, \\ a_k + b_{k+1} - b_k, & 1 \le k \le j-1, \\ a_j - b_j, & k = j, \end{cases} \tag{9} $$

with $a_0 = \sigma^{1-\mu}$,

$$a_k = (k+\sigma)^{1-\mu} - (k+\sigma-1)^{1-\mu}, k \geq 1, \tag{10}$$

$$b_k = \frac{1}{2-\mu}\left[(k+\sigma)^{2-\mu} - (k+\sigma-1)^{2-\mu}\right] - \frac{1}{2}\left[(k+\sigma)^{1-\mu} + (k+\sigma-1)^{1-\mu}\right], k \geq 1. \tag{11}$$

Lemma 2.1.1. *([25]) The coefficients w_k satisfy*

(a). $w_0 > w_1 > \cdots > w_j > 0, j \geq 1.$

(b). $w_j > \frac{1-\mu}{2(j+\sigma)^{\mu}}, j \geq 0.$

(c). $(2\sigma-1)w_0 - \sigma w_1 > 0.$

2.2 | The spatial discretization

In this subsection, we will introduce two high-order schemes for the spatial discretization of (5)–(7). For this end, let N_x be a positive integer. We divide the interval $[0, b]$ into N_x subintervals with $\Omega_x : 0 = x_0 < x_1 < \cdots < x_{N_x} = b$. Suppose $x_i = ih$, with the mesh width $h = \frac{b}{N_x}$. Let $u(x,t)$ denote the exact solution of problem (5)–(7). For $0 \leq i \leq N_x$ and $0 \leq j \leq N_t$, we shall use the notation $u_i^j = u(x_i, t_j)$ and $F_i^j = F(x_i, t_j)$. Further, let U_i^j denote the approximation of u_i^j. Now, let $D_h = \{y|(y_0, y_1, \cdots, y_{N_x})\}$ and $D_h^* = \{y|(y_0, y_1, \cdots, y_{N_x}), y_0 = y_{N_x} = 0\}$. For any grid function $y \in D_h$, let us denote

$$\delta_x y_{i+\frac{1}{2}} = \frac{1}{h}(y_{i+1} - y_i), \qquad \delta_x^2 y_i = \frac{1}{h}\left(\delta_x y_{i+\frac{1}{2}} - \delta_x y_{i-\frac{1}{2}}\right),$$

$$\delta_x^3 y_{i+\frac{1}{2}} = \frac{1}{h}(\delta_x^2 y_{i+1} - \delta_x^2 y_i), \qquad \delta_x^4 y_i = \frac{1}{h}\left(\delta_x^3 y_{i+\frac{1}{2}} - \delta_x^3 y_{i-\frac{1}{2}}\right).$$

2.2.1 | $\mathrm{CFD}_{g-\sigma}$ scheme

Here, we introduce a high order compact scheme ($\mathrm{CFD}_{g-\sigma}$) for the spatial discretization of (5)–(7). Now for any grid function $y \in D_h$, the compact differential operator (H_c) is defined as

$$H_c y_i = \begin{cases} \frac{1}{12}y_{i-1} + \frac{10}{12}y_i + \frac{1}{12}y_{i+1}, & 1 \leq i \leq N_x - 1, \\ y_i, & i = 0 \text{ or } N_x. \end{cases} \tag{12}$$

Also, here it is evident that

$$H_c y_i = \left(I + \frac{h^2}{12}\delta_x^2\right) y_i, 1 \leq i \leq N_x - 1. \tag{13}$$

Lemma 2.2.1. *([29]) Suppose $\psi(x) \in C^6[x_{i-1}, x_{i+1}]$ and $\tilde{\phi}(s) = -3(1-s)^5 + 5(1-s)^3$. Then*

$$\frac{1}{12}\psi''(x_{i-1}) + \frac{10}{12}\psi''(x_i) + \frac{1}{12}\psi''(x_{i+1}) = \frac{\psi(x_{i-1}) - 2\psi(x_i) + \psi(x_{i+1})}{h^2} + \frac{h^4}{360}\int_0^1 \left(\psi^{(6)}(x_i - sh) + \psi^{(6)}(x_i + sh)\right)\tilde{\phi}(s)ds.$$

Now consider problem (5) at $(x_i, t_{j+\sigma})$, $0 \leq i \leq N_x, 0 \leq j \leq N_t - 1$. We have

$${}_0^C D_{t:[\chi(t),1]}^{\mu} u(x_i, t_{j+\sigma}) + q(t_{j+\sigma})u(x_i, t_{j+\sigma}) = p(t_{j+\sigma})\frac{\partial^2 u(x_i, t_{j+\sigma})}{\partial x^2} + F(x_i, t_{j+\sigma}). \tag{14}$$

Lemma 2.2.2. *([25]) If $W(t) \in C^2[0,T]$, then on the nonuniform mesh Ω_t, we have*

$$W(t_{j+\sigma_j}) \equiv \sigma_j W(t_{j+1}) + (1-\sigma_j)W(t_j) = W(t_{j+\sigma}) + O(\widetilde{\Delta}t^2),$$

where $\sigma = 1 - \frac{\mu}{2}$, $\sigma_j = \frac{t_{j+\sigma}-t_j}{t_{j+1}-t_j} \in (0,1)$, *and* $\widetilde{\Delta}t = \max_{0\le j\le N_t-1}(t_{j+1}-t_j)$.

Now, in order to derive the $\mathrm{CFD}_{g-\sigma}$ scheme, we use the $gL2-1_\sigma$ approximation of GFD given in Equation (8) and apply the compact operator H_c defined in Equation (12) to both sides of Equation (14). Further, we approximate $u_i^{j+\sigma}$ (and similarly $u_{i-1}^{j+\sigma}$, $u_{i+1}^{j+\sigma}$) by Lemma 2.2.2. We obtain

$$\nu H_c\left[w_0 u_i^{j+1} - \sum_{k=1}^{j}(w_{j-k}-w_{j-k+1})u_i^k - w_j u_i^0\right] + q^{j+\sigma}H_c u_i^{j+\sigma_j} = p^{j+\sigma}\delta_x^2 u_i^{j+\sigma_j} + H_c F_i^{j+\sigma} + {}_cR_i^{j+\sigma}, 1 \le i \le N_x-1, \tag{15}$$

$$u_i^0 = g(x_i), 1 \le i \le N_x - 1, \tag{16}$$

$$u_0^j = \phi_1(t_j), u_{N_x}^j = \phi_2(t_j), 1 \le j \le N_t, \tag{17}$$

where $q^{j+\sigma} = q(t_{j+\sigma})$ and $p^{j+\sigma} = p(t_{j+\sigma})$. Further, removing the truncation error term ${}_cR_i^{j+\sigma} = O(\Delta t^{3-\mu}, \widetilde{\Delta}t^2, h^4)$ from Equation (15), we have

$$\nu H_c\left[w_0 U_i^{j+1} - \sum_{k=1}^{j}(w_{j-k}-w_{j-k+1})U_i^k - w_j U_i^0\right] + q^{j+\sigma}H_c U_i^{j+\sigma_j} = p^{j+\sigma}\delta_x^2 U_i^{j+\sigma_j} + H_c F_i^{j+\sigma}, 1 \le i \le N_x-1, \tag{18}$$

$$U_i^0 = g(x_i), 1 \le i \le N_x - 1, \tag{19}$$

$$U_0^j = \phi_1(t_j), U_{N_x}^j = \phi_2(t_j), 1 \le j \le N_t. \tag{20}$$

Thus, we can recursively solve the discrete scheme (18)–(20) for U_i^j, $1 \le i \le N_x-1$, $1 \le j \le N_t$ and obtain the numerical solution of problem (5)–(7).

2.2.2 | $\mathrm{PQS}_{g-\sigma}$ scheme

Here, we introduce a high order parametric quintic spline operator H_q, which plays a vital role in obtaining the high order spatial discretized scheme for (5)–(7).

Definition 2.1 ([43, 47, 48])**.** A function $P_{\Omega_x}(x;\eta) \in C^4[0,b]$ for a given mesh Ω_x is said to be the parametric quintic spline with parameter $\eta > 0$ if its restriction $P_{\Omega_x,i}(x;\eta) = \{P_{\Omega_x}(x;\eta)\}_{[x_{i-1},x_i]}$, $1 \le i \le N_x$ fulfills the condition $P_{\Omega_x,i}(x_l) = y_l$, $l = i-1, i$ and

$$P_{\Omega_x,i}^{(4)}(x) + \eta^2 P_{\Omega_x,i}''(x) = (f_i + \eta^2\bar{w}_i)\frac{(x-x_{i-1})}{h} + (f_{i-1} + \eta^2\bar{w}_{i-1})\frac{(x_i-x)}{h}, \tag{21}$$

where $P_{\Omega_x,i}''(x_l) = \bar{w}_l$ and $P_{\Omega_x,i}^{(4)}(x_l) = f_l$, $l = i-1, i$.

Solving Equation (21) for $P_{\Omega_x,i}$ yields

$$\begin{aligned} P_{\Omega_x,i}(x) = {} & \gamma y_i + \bar{\gamma} y_{i-1} + \frac{h^2}{6}(S_1(\gamma)\bar{w}_i + S_1(\bar{\gamma})\bar{w}_{i-1}) + \left(\frac{h}{\tilde{\nu}}\right)^4\left(\frac{\tilde{\nu}^2}{6}S_1(\gamma) - S_2(\gamma)\right)f_i \\ & + \left(\frac{h}{\tilde{\nu}}\right)^4\left(\frac{\tilde{\nu}^2}{6}S_1(\bar{\gamma}) - S_2(\bar{\gamma})\right)f_{i-1}, \end{aligned} \tag{22}$$

where $\tilde{\nu} = \eta h$, $\gamma = \frac{(x-x_{i-1})}{h}$, $\bar{\gamma} = 1-\gamma$, $S_1(\gamma) = \gamma^3 - \gamma$, and $S_2(\gamma) = \gamma - \frac{\sin\tilde{\nu}\gamma}{\sin\tilde{\nu}}$.

Now using the continuity conditions of the first and third derivatives of $P_{\Omega_x}(x)$ at $x = x_i$, namely, $P'_{\Omega_x,i}(x_i) = P'_{\Omega_x,i+1}(x_i)$ and $P''_{\Omega_x,i}(x_i) = P''_{\Omega_x,i+1}(x_i)$, we have two relations including y_l, $\bar{w}_l$, and f_l, $l = i-1, i, i+1$. After the elimination of f_l, we get

$$\bar{p}\bar{w}_{i-2}+\bar{q}\bar{w}_{i-1}+\bar{s}\bar{w}_i+\bar{q}\bar{w}_{i+1}+\bar{p}\bar{w}_{i+2}=(\delta_x^2+\alpha h^2\delta_x^4)y_i, 2\le i\le N_x-2, \tag{23}$$

where $\alpha = \frac{1}{\tilde{v}^2}\left(\frac{\tilde{v}}{\sin\tilde{v}} - 1\right)$ and $\bar{p}$, $\bar{q}$, and $\bar{s}$ such that $2\bar{p} + 2\bar{q} + \bar{s} = 1$.

We can only consider $\alpha \in \left(0, \frac{1}{2}\right)$, due to the consistency relation given in [43, 46]. But using α in $\left(0, \frac{1}{2}\right)$ provides various schemes with different accuracy.

Apart from Equation (23), we require two more equations, which can be obtained from the following formulation:

$$-\tilde{R}_i = \frac{a_{i-1}y_{i-1} + a_i y_i + a_{i+1}y_{i+1}}{h^2} + a^*_{i-1}\bar{w}_{i-1} + a^*_i\bar{w}_i + a^*_{i+1}\bar{w}_{i+1}, i = 1, N_x - 1.$$

Here, $\tilde{R}_i$ denotes the local truncation error at $x = x_i$. Further, a's and a^*'s are the unknown coefficients, which are required to be evaluated in such a way that $\tilde{R}_i = O(h^4)$ for $i = 1, N_x - 1$.

Now in the above two equations at $x = x_i$, we carry out Taylor expansions and take $\tilde{R}_i = O(h^4)$ for $i = 1, N_x - 1$ to get

$$\left(a_{i-1}, a_i, a_{i+1}, a^*_{i-1}, a^*_i, a^*_{i+1}\right) = \left(-1, 2, -1, \frac{1}{12}, \frac{10}{12}, \frac{1}{12}\right), i = 1, N_x - 1.$$

Next, removing the local truncation error term $\tilde{R}_i$, we get the following equations:

$$\left(I + \frac{h^2}{12}\delta_x^2\right)\bar{w}_i = \delta_x^2 y_i, i = 1, N_x - 1. \tag{24}$$

Thus, combining (23) and (24), we define the parametric quintic spline operator H_q as follows:

$$H_q y_i = \begin{cases} \left(I + \frac{h^2}{12}\delta_x^2\right) y_i, & i = 1, N_x - 1, \\ \bar{p}y_{i-2} + \bar{q}y_{i-1} + \bar{s}y_i + \bar{q}y_{i+1} + \bar{p}y_{i+2}, & 2 \le i \le N_x - 2. \end{cases} \tag{25}$$

Also, for $\alpha \in \left(0, \frac{1}{2}\right)$, we introduce the notation

$$\tilde{\delta}_x^2 y_i = \begin{cases} \delta_x^2 y_i, & i = 1, N_x - 1, \\ \left(\delta_x^2 + \alpha h^2\delta_x^4\right) y_i, & 2 \le i \le N_x - 2. \end{cases} \tag{26}$$

Now we use Taylor expansions at $x = x_i$ and get the following result.

Lemma 2.2.3. *Suppose $y \in C^8[0, b]$. If*

$$\bar{p} = \frac{\alpha}{12} - \frac{1}{240}, \bar{q} = \frac{8\alpha}{12} + \frac{1}{10}, \bar{s} = -\frac{3\alpha}{2} + \frac{97}{120}, \tag{27}$$

then the following result holds:

$$H_q\frac{\partial^2 y}{\partial x^2}\Big|_{x_i} - \tilde{\delta}_x^2 y_i = \begin{cases} -\frac{h^4}{240}\frac{\partial^6 y}{\partial x^6}\Big|_{x_i} + O(h^6), & i = 1, N_x - 1, \\ \tilde{Q}h^6\frac{\partial^8 y}{\partial x^8}\Big|_{x_i} + O(h^8), & 2 \le i \le N_x - 2, \end{cases} \tag{28}$$

where $Q = -\frac{8\bar{p}}{45} - \frac{\bar{q}}{360} + \frac{126\alpha}{10080} + \frac{1}{20160}$ and $\alpha \in \left(0, \frac{1}{2}\right)$.

Remark 2.2. We fix the values of $\bar{p}$, $\bar{q}$, and $\bar{s}$ as given in Equation (27) for the rest of the paper.

Now we consider problem (5) at $(x_i, t_{j+\sigma})$, $0 \le i \le N_x, 0 \le j \le N_t - 1$. We have

$$ {}_0^C D^{\mu}_{t:[z(t),1]} u(x_i, t_{j+\sigma}) + q(t_{j+\sigma}) u(x_i, t_{j+\sigma}) = p(t_{j+\sigma}) \frac{\partial^2 u(x_i, t_{j+\sigma})}{\partial x^2} + F(x_i, t_{j+\sigma}). \tag{29} $$

The $\mathrm{PQS}_{g-\sigma}$ scheme is obtained using the $gL2-1_\sigma$ approximation of GFD given in Equation (8), parametric quintic spline operator H_q defined in Equation (25), and Lemma 2.2.2 into Equation (29). We obtain

$$ \nu H_q \left[w_0 u_i^{j+1} - \sum_{k=1}^{j} (w_{j-k} - w_{j-k+1}) u_i^k - w_j u_i^0 \right] + q^{j+\sigma} H_q u_i^{j+\sigma_j} = p^{j+\sigma} \tilde{\delta}_x^2 u_i^{j+\sigma_j} + H_q F_i^{j+\sigma} + {}_q R_i^{j+\sigma}, 1 \le i \le N_x - 1, \tag{30} $$

$$ u_i^0 = g(x_i), 1 \le i \le N_x - 1, \tag{31} $$

$$ u_0^j = \phi_1(t_j), u_{N_x}^j = \phi_2(t_j), 1 \le j \le N_t, \tag{32} $$

where $q^{j+\sigma} = q(t_{j+\sigma})$ and $p^{j+\sigma} = p(t_{j+\sigma})$. Further, in view of Equation (30), removing the truncation error term ${}_q R_i^{j+\sigma}$, we have

$$ \nu H_q \left[w_0 U_i^{j+1} - \sum_{k=1}^{j} (w_{j-k} - w_{j-k+1}) U_i^k - w_j U_i^0 \right] + q^{j+\sigma} H_q U_i^{j+\sigma_j} = p^{j+\sigma} \tilde{\delta}_x^2 U_i^{j+\sigma_j} + H_q F_i^{j+\sigma}, 1 \le i \le N_x - 1, \tag{33} $$

$$ U_i^0 = g(x_i), 1 \le i \le N_x - 1, \tag{34} $$

$$ U_0^j = \phi_1(t_j), U_{N_x}^j = \phi_2(t_j), 1 \le j \le N_t. \tag{35} $$

Thus, we can recursively solve the scheme (33)–(35) for U_i^j, $1 \le i \le N_x - 1$, $1 \le j \le N_t$, and obtain the numerical solution of problem (5)–(7).

3 | STABILITY AND CONVERGENCE ANALYSIS

In this section, we provide stability and convergence analysis of the schemes $\mathrm{CFD}_{g-\sigma}$ and $\mathrm{PQS}_{g-\sigma}$. So, first, we define some notation and give a few lemmas, which will be useful for the analysis of both schemes.

For any $\bar{u}, \bar{v} \in D_h^*$, we define the discrete inner product, L_2 norm, H^1 seminorm, and L_∞ norm as follows:

$$ < \bar{u}, \bar{v} >= h \sum_{i=1}^{N_x - 1} \bar{u}_i \cdot \bar{v}_i, \|\bar{u}\| = \sqrt{< \bar{u}, \bar{u} >}, $$

$$ \|\delta_x \bar{u}\| = \sqrt{h \sum_{i=1}^{N_x} \left(\delta_x \bar{u}_{i-\frac{1}{2}} \right)^2}, \|\bar{u}\|_\infty = \max_{1 \le i \le N_x - 1} |\bar{u}_i|. $$

Similarly, we can define $\|\delta_x^2 \bar{u}\|$, $\|H_c \bar{u}\|$, and $\|H_q \bar{u}\|$.

Lemma 3.1. *([25]) For the numbers r_m, $0 \le m \le j+1$, the following inequalities hold:*

$$ r_{j+1} \sum_{k=0}^{j} (r_{k+1} - r_k) w_{j-k} \ge \frac{1}{2} \sum_{k=0}^{j} \left((r_{k+1})^2 - (r_k)^2 \right) w_{j-k} + \frac{1}{2w_0} \left(\sum_{k=0}^{j} (r_{k+1} - r_k) w_{j-k} \right)^2, $$

$$ r_j \sum_{k=0}^{j} (r_{k+1} - r_k) w_{j-k} \ge \frac{1}{2} \sum_{k=0}^{j} \left((r_{k+1})^2 - (r_k)^2 \right) w_{j-k} - \frac{1}{2(w_0 - w_1)} \left(\sum_{k=0}^{j} (r_{k+1} - r_k) w_{j-k} \right)^2. $$

Lemma 3.2 ([25]). *If the inverse of the scale function z is concave, then for the numbers r_m, $0 \le m \le j+1$, the following inequality holds:*

$$\{\sigma_j r_{j+1} + (1-\sigma_j) r_j\} \sum_{k=0}^{j} (r_{k+1} - r_k) w_{j-k} \ge \frac{1}{2} \sum_{k=0}^{j} \left((r_{k+1})^2 - (r_k)^2 \right) w_{j-k},$$

where $\sigma_j = \frac{t_{j+\sigma} - t_j}{t_{j+1} - t_j} \in (0,1)$.

3.1 | Stability and convergence analysis of $\mathrm{CFD}_{g-\sigma}$ scheme

In this subsection, we provide stability and convergence analysis of $\mathrm{CFD}_{g-\sigma}$ scheme (18)-(20).

Let $\tilde{u}_i^j$ solve the following problem

$$\nu H_c \left[w_0 \tilde{u}_i^{j+1} - \sum_{k=1}^{j} (w_{j-k} - w_{j-k+1}) \tilde{u}_i^k - w_j \tilde{u}_i^0 \right] + q^{j+\sigma} H_c \tilde{u}_i^{j+\sigma_j} = p^{j+\sigma} \delta_x^2 \tilde{u}_i^{j+\sigma_j} + H_c \hat{F}_i^{j+\sigma}, 1 \le i \le N_x - 1, \tag{36}$$

$$\tilde{u}_i^0 = \hat{g}(x_i), 1 \le i \le N_x - 1, \tag{37}$$

$$\tilde{u}_0^j = \phi_1(t_j), \tilde{u}_{N_x}^j = \phi_2(t_j), 1 \le j \le N_t. \tag{38}$$

Suppose $e_i^j = \tilde{u}_i^j - U_i^j$. Then, from equations (18)-(20) and (36)-(38), it is evident that $e_i^j \in D_h^*$ and solves the following linear system

$$\nu H_c \left[w_0 e_i^{j+1} - \sum_{k=1}^{j} (w_{j-k} - w_{j-k+1}) e_i^k - w_j e_i^0 \right] + q^{j+\sigma} H_c e_i^{j+\sigma_j} = p^{j+\sigma} \delta_x^2 e_i^{j+\sigma_j} + H_c \tilde{F}_i^{j+\sigma}, 1 \le i \le N_x - 1, \tag{39}$$

$$e_i^0 = \hat{g}(x_i) - g(x_i), 1 \le i \le N_x - 1, \tag{40}$$

$$e_0^j = 0, e_{N_x}^j = 0, 1 \le j \le N_t, \tag{41}$$

where $\tilde{F}_i^{j+\sigma} = \hat{F}_i^{j+\sigma} - F_i^{j+\sigma}$. Now we will prove a result that will directly show the stability of $\mathrm{CFD}_{g-\sigma}$ scheme (18)-(20).

Theorem 3.3. *Suppose the inverse of the scale function z is concave. Then, the solution to the discrete problem (39)–(41) satisfies*

$$\|e^{j+1}\|^2 \le \frac{12}{5} \left[\|H_c e^0\|^2 + C \max_{0 \le l \le N_t - 1} \|H_c \tilde{F}^{l+\sigma}\|^2 \right], \tag{42}$$

where $C = \frac{(z(T) - z(0))^{\mu} \Gamma(1-\mu)}{\epsilon}$ *and* $\epsilon = \frac{8 p^{j+\sigma}}{3b} > 0$.

Proof. Multiplying Equation (39) with $h H_c e_i^{j+\sigma_j}$ and then summing from $i = 1$ to $N_x - 1$, we get

$$\begin{aligned} &\nu \left[w_0 (H_c e^{j+\sigma_j}, H_c e^{j+1}) - \sum_{k=1}^{j} (w_{j-k} - w_{j-k+1}) (H_c e^{j+\sigma_j}, H_c e^k) - w_j (H_c e^{j+\sigma_j}, H_c e^0) \right] \\ &= p^{j+\sigma} (H_c e^{j+\sigma_j}, \delta_x^2 e^{j+\sigma_j}) - q^{j+\sigma} (H_c e^{j+\sigma_j}, H_c e^{j+\sigma_j}) + (H_c e^{j+\sigma_j}, H_c \hat{F}^{j+\sigma}). \end{aligned} \tag{43}$$

Now applying Lemma 3.2 to the left side of the equation gives

$$\begin{aligned} & w_0(H_c e^{j+\sigma_j}, H_c e^{j+1}) - \sum_{k=1}^{j}(w_{j-k} - w_{j-k+1})(H_c e^{j+\sigma_j}, H_c e^{k}) - w_j(H_c e^{j+\sigma_j}, H_c e^{0}) \\ & \geq \frac{1}{2}\left[w_0\|H_c e^{j+1}\|^2 - \sum_{k=1}^{j}(w_{j-k} - w_{j-k+1})\|H_c e^{k}\|^2 - w_j\|H_c e^{0}\|^2 \right]. \end{aligned} \tag{44}$$

Next,

$$\begin{aligned} (H_c e^{j+\sigma_j}, \delta_x^2 e^{j+\sigma_j}) &= (e^{j+\sigma_j}, \delta_x^2 e^{j+\sigma_j}) + \frac{h^2}{12}(\delta_x^2 e^{j+\sigma_j}, \delta_x^2 e^{j+\sigma_j}) \\ &\leq -h\sum_{i=0}^{N_x-1}\left(\delta_x e^{j+\sigma_j}_{i+\frac{1}{2}}\right)^2 + \frac{h}{6}\left[\sum_{i=1}^{N_x-1}\left(\delta_x e^{j+\sigma_j}_{i+\frac{1}{2}}\right)^2 + \sum_{i=1}^{N_x-1}\left(\delta_x e^{j+\sigma_j}_{i-\frac{1}{2}}\right)^2\right] \\ &\quad \left(\text{since } \; h^2\left(\delta_x^2 e_i^{j+\sigma_j}\right)^2 \leq 2\left(\delta_x e^{j+\sigma_j}_{i+\frac{1}{2}}\right)^2 + 2\left(\delta_x e^{j+\sigma_j}_{i-\frac{1}{2}}\right)^2\right) \\ &\leq -\frac{2}{3}\sum_{i=0}^{N_x-1} h\left(\delta_x e^{j+\sigma_j}_{i+\frac{1}{2}}\right)^2 \text{(using discrete Poincare inequality)} \\ &\leq -\frac{8}{3b}\|e^{j+\sigma_j}\|^2. \end{aligned} \tag{45}$$

Moreover, for $\epsilon = \frac{8p^{j+\sigma}}{3b} > 0$, Young's inequality yields

$$\begin{aligned} (H_c e^{j+\sigma_j}, H_c \hat{F}^{j+\sigma}) &\leq \epsilon\|H_c e^{j+\sigma_j}\|^2 + \frac{1}{4\epsilon}\|H_c \tilde{F}^{j+\sigma}\|^2 \\ &= h\epsilon\sum_{i=1}^{N_x-1}\left(\frac{e^{j+\sigma_j}_{i-1} + 10e_i^{j+\sigma_j} + e^{j+\sigma_j}_{i+1}}{12}\right)^2 + \frac{1}{4\epsilon}\|H_c \tilde{F}^{j+\sigma}\|^2 \\ &= \frac{8p^{j+\sigma}}{3b}\|e^{j+\sigma_j}\|^2 + \frac{3b}{32p^{j+\sigma}}\|H_c \tilde{F}^{j+\sigma}\|^2. \end{aligned} \tag{46}$$

Now the use of the inequalities (44), (45) and (46) in Equation (43) yields

$$w_0\|H_c e^{j+1}\|^2 - \sum_{k=1}^{j}(w_{j-k} - w_{j-k+1})\|H_c e^{k}\|^2 - w_j\|H_c e^{0}\|^2 \leq \frac{3b}{16\nu p^{j+\sigma}}\|H_c \tilde{F}^{j+\sigma}\|^2,$$

which gives

$$w_0\|H_c e^{j+1}\|^2 - \sum_{k=1}^{j}(w_{j-k} - w_{j-k+1})\|H_c e^{k}\|^2 \leq w_j\left[\|H_c e^{0}\|^2 + \frac{3b}{16\nu p^{j+\sigma} w_j}\|H_c \tilde{F}^{j+\sigma}\|^2\right].$$

Thus, using Lemma 2.1.1 and noting that $(j+\sigma)\Delta t = \frac{(j+\sigma)(z(T)-z(0))}{N_t} < (z(T) - z(0))$, we get

$$w_0\|H_c e^{j+1}\|^2 - \sum_{k=1}^{j}(w_{j-k} - w_{j-k+1})\|H_c e^{k}\|^2 \leq w_j\chi, \tag{47}$$

where

$$\chi = \|H_c e^{0}\|^2 + \frac{\Gamma(1-\mu)(z(T) - z(0))^{\mu}}{\epsilon}\max_{0\leq l\leq N_t-1}\|H_c \tilde{F}^{l+\sigma}\|^2.$$

Now we prove by induction that

$$\|H_c e^{j+1}\|^2 \leq \chi, 0 \leq j \leq N_t - 1. \tag{48}$$

Putting $j = 0$ in Equation (47) we get

$$\|H_c e^1\|^2 \leq \chi,$$

which is identical to (48) for $j = 0$. Let us assume that (48) holds for $j = 0, 1, \ldots, n-1$, that is

$$\|H_c e^{j+1}\|^2 \leq \chi, 0 \leq j \leq n - 1. \tag{49}$$

Now using $j = n$ in the inequality (47) together with the assumption (49) we get

$$w_0\|H_c e^{n+1}\|^2 \leq \sum_{k=1}^{n}(w_{n-k} - w_{n-k+1})\|H_c e^k\|^2 + w_n\chi \leq \left[\sum_{k=1}^{n}(w_{n-k} - w_{n-k+1}) + w_n\right]\chi = w_0\chi.$$

Thus, (49) holds for all j. Since the norms $\|H_c e\|$ and $\|e\|$ are equivalent from the inequalities

$$\frac{5}{12}\|e\| \leq \|H_c e\| \leq \|e\|. \tag{50}$$

Thus, (42) follows from (48) and the first inequality in (50). □

Now we will prove the main convergence theorem.

Theorem 3.4. *Let $u(x,t) \in C^{6,2}([0,b]\times[0,T])$ be the solution of problem (5)–(7), $u(x, \mathcal{Z}^{-1}(z)) \in C^3[z(T) - z(0)]$ for any fixed x, inverse of z is concave, and $\{U_i^j, 0 \leq i \leq N_x, 1 \leq j \leq N_t\}$ be the solution of the discrete problem (18)–(20). Then, the following result holds*

$$\|u_i^{j+1} - U_i^{j+1}\| \leq \bar{c}O(\Delta t^{3-\mu}, \widetilde{\Delta} t^2, h^4),$$

where $\bar{c} = \sqrt{\frac{12(z(T)-z(0))^\mu\Gamma(1-\mu)}{5\epsilon}}$ *and* $\epsilon = \frac{8p^{j+\sigma}}{3b}$.

Proof. Let $\xi_i^{j+1} = u_i^{j+1} - U_i^{j+1}$. Now subtracting the linear system (18)–(20) from (15)–(17), we get

$$\nu H_c\left[w_0\xi_i^{j+1} - \sum_{k=1}^{j}(w_{j-k} - w_{j-k+1})\xi_i^k - w_j\xi_i^0\right] + q^{j+\sigma}H_c\xi_i^{j+\sigma_j} = p^{j+\sigma}\delta_x^2\xi_i^{j+\sigma_j} + {}_cR_i^{j+\sigma}, 1 \leq i \leq N_x - 1, \tag{51}$$

$$\xi_i^0 = 0, 1 \leq i \leq N_x - 1, \tag{52}$$

$$\xi_0^j = 0, \xi_{N_x}^j = 0, 1 \leq j \leq N_t. \tag{53}$$

Since $\xi_i^{j+1} \in D_h^*$, therefore applying Theorem 3.3 for the error equation (51)–(53) we have

$$\|\xi^{j+1}\|^2 \leq \tilde{C}\max_{0\leq l\leq N_t-1}\|{}_cR^{l+\sigma}\|^2, 0 \leq j \leq N_t - 1, \tag{54}$$

where $\tilde{C} = \frac{12(z(T)-z(0))^\mu\Gamma(1-\mu)}{5\epsilon}$ and $\epsilon = \frac{8p^{j+\sigma}}{3b}$.

Since we have the following truncation error bound

$$\max_{0\le l\le N_t-1} \|{}_cR^{l+\sigma}\| = O(\Delta t^{3-\mu}, \widetilde{\Delta} t^2, h^4),$$

therefore using it in Equation (54) proves the theorem. □

3.2 | Stability and convergence analysis of $PQS_{g-\sigma}$ scheme

In this subsection, we provide stability and convergence analysis of $PQS_{g-\sigma}$ scheme (33)-(35). We shall use the following lemmas.

Lemma 3.5. *[49] Let $V \in D_h^*$. If $\alpha \in \left(0, \frac{67}{492}\right)$, then*

$$\Upsilon^2(V,V) \le (H_qV, H_qV) \le \left(\frac{60}{61}\right)^2 (V,V),$$

where $\Upsilon > 0$ is given by

$$\Upsilon = \begin{cases} -\frac{71\alpha}{24} + \frac{283}{480}, & 0 < \alpha \le \frac{1}{20}, \\ -\frac{9\alpha}{2} + \frac{2}{3}, & \alpha = \frac{1}{20}, \\ -\frac{41\alpha}{8} + \frac{67}{96}, & \frac{1}{20} < \alpha < \frac{67}{492}. \end{cases}$$

Lemma 3.6. *[49] Let $V \in D_h^*$. If $\alpha \in (0, \rho_0)$, where $\rho_0 = \frac{-161+12\sqrt{229}}{340}$, then*

$$(H_qV, \tilde{\delta}_x^2 V) \le -\frac{4\Upsilon_1}{b}(V,V),$$

where $\Upsilon_1 > 0$ is given by

$$\Upsilon_1 = \begin{cases} \frac{71}{120} - 7\alpha + 18\alpha^2, & 0 < \alpha < \rho_1, \\ \frac{2}{3} - 10\alpha, & \alpha = \rho_1, \\ \frac{83}{120} - 11\alpha - 6\alpha^2, & \rho_1 < \alpha \le \frac{1}{20}, \\ \frac{83}{120} - \frac{1288\alpha}{120} - \frac{1360\alpha^2}{120}, & \frac{1}{20} < \alpha < \rho_0. \end{cases}$$

Here, $\rho_0 = \frac{-161+12\sqrt{229}}{340}$ and $\rho_1 = \frac{-5+2\sqrt{10}}{60}$.

Let $\tilde{u}_i^j$ solve the following problem

$$\nu H_q \left[w_0 \tilde{u}_i^{j+1} - \sum_{k=1}^{j} (w_{j-k} - w_{j-k+1}) \tilde{u}_i^k - w_j \tilde{u}_i^0 \right] + q^{j+\sigma} H_q \tilde{u}_i^{j+\sigma_j} = p^{j+\sigma} \tilde{\delta}_x^2 \tilde{u}_i^{j+\sigma_j} + H_q \hat{F}_i^{j+\sigma}, 1 \le i \le N_x - 1, \tag{55}$$

$$\tilde{u}_i^0 = \hat{g}(x_i), 1 \le i \le N_x - 1, \tag{56}$$

$$\tilde{u}_0^j = \phi_1(t_j), \tilde{u}_{N_x}^j = \phi_2(t_j), 1 \le j \le N_t. \tag{57}$$

Now, let $e_i^j = \tilde{u}_i^j - U_i^j$. Then, from equations (33)-(35) and (55)-(57), it is evident that $e_i^j \in D_h^*$ and solves the following linear system

$$\nu H_q \left[w_0 e_i^{j+1} - \sum_{k=1}^{j} (w_{j-k} - w_{j-k+1}) e_i^k - w_j e_i^0 \right] + q^{j+\sigma} H_q e_i^{j+\sigma_j} = p^{j+\sigma} \tilde{\delta}_x^2 e_i^{j+\sigma_j} + H_q \tilde{F}_i^{j+\sigma}, 1 \le i \le N_x - 1, \tag{58}$$

$$e_i^0 = \hat{g}(x_i) - g(x_i), 1 \le i \le N_x - 1, \tag{59}$$

$$e_0^j = 0, e_{N_x}^j = 0, 1 \le j \le N_t, \tag{60}$$

where $\tilde{F}_i^{j+\sigma} = \hat{F}_i^{j+\sigma} - F_i^{j+\sigma}$. Next, we will prove a result that will directly show the stability of the scheme.

Theorem 3.7. *Suppose the inverse of the scale function z is concave. If $\alpha \in (0, \rho_0)$, then the solution of the discrete problem (58)–(60) satisfies*

$$\|e^{j+1}\|^2 \le \tilde{c}\left[\|H_q e^0\|^2 + \frac{\Gamma(1-\mu)(z(T)-z(0))^\mu}{\tilde{\epsilon}} \max_{0\le l\le N_t-1} \|H_q \tilde{F}^{l+\sigma}\|^2\right], \tag{61}$$

where $\tilde{c} = \frac{1}{\Upsilon^2}$ *and* $\tilde{\epsilon} = \left(\frac{61}{60}\right)^2 \frac{4\Upsilon_1 p^{j+\sigma}}{b} > 0$.

Proof. Multiplying Equation (58) with $hH_q e_i^{j+\sigma_j}$ and then summing from $i = 1$ to $N_x - 1$, we get

$$\begin{aligned} &\nu\left[w_0(H_q e^{j+\sigma_j}, H_q e^{j+1}) - \sum_{k=1}^{j}(w_{j-k} - w_{j-k+1})(H_q e^{j+\sigma_j}, H_q e^k) - w_j(H_q e^{j+\sigma_j}, H_q e^0)\right] \\ =&p^{j+\sigma}(H_q e^{j+\sigma_j}, \tilde{\delta}_x^2 e^{j+\sigma_j}) - q^{j+\sigma}(H_q e^{j+\sigma_j}, H_q e^{j+\sigma_j}) + (H_q e^{j+\sigma_j}, H_q \hat{F}^{j+\sigma}), \end{aligned} \tag{62}$$

Next, applying Lemma 3.2 to the left side of the above equation gives

$$\begin{aligned} &w_0(H_q e^{j+\sigma_j}, H_q e^{j+1}) - \sum_{k=1}^{j}(w_{j-k} - w_{j-k+1})(H_q e^{j+\sigma_j}, H_q e^k) - w_j(He^{j+\sigma_j}, H_q e^0) \\ \ge& \frac{1}{2}\left[w_0\|H_q e^{j+1}\|^2 - \sum_{k=1}^{j}(w_{j-k} - w_{j-k+1})\|H_q e^k\|^2 - w_j\|H_q e^0\|^2\right]. \end{aligned} \tag{63}$$

Since $e^j \in D_h^*$, using Lemma 3.6 for the term $(H_q e^{j+\sigma_j}, \tilde{\delta}_x^2 e^{j+\sigma_j})$ we have

$$(H_q e^{j+\sigma_j}, \tilde{\delta}_x^2 e^{j+\sigma_j}) \le -\frac{4\Upsilon_1}{b}(e^{j+\sigma_j}, e^{j+\sigma_j}). \tag{64}$$

Moreover, for any $\tilde{\epsilon} > 0$, applying Young's inequality and Lemma 3.5 to the term $(H_q e^{j+\sigma_j}, H_q \hat{F}^{j+\sigma})$ yields

$$(H_q e^{j+\sigma_j}, H_q \hat{F}^{j+\sigma}) \le \tilde{\epsilon}\|H_q e^{j+\sigma_j}\|^2 + \frac{1}{4\tilde{\epsilon}}\|H_q \tilde{F}^{j+\sigma}\|^2 \le \tilde{\epsilon}\left(\frac{60}{61}\right)^2 \|e^{j+\sigma_j}\|^2 + \frac{1}{4\tilde{\epsilon}}\|H_q \tilde{F}^{j+\sigma}\|^2. \tag{65}$$

Now, setting $\tilde{\epsilon} = \left(\frac{61}{60}\right)^2 \frac{4\Upsilon_1 p^{j+\sigma}}{b} > 0$ and using the inequalities (63), (64) and (65) in Equation (62) yields

$$w_0\|H_q e^{j+1}\|^2 - \sum_{k=1}^{j}(w_{j-k} - w_{j-k+1})\|H_q e^k\|^2 - w_j\|H_q e^0\|^2 \le \frac{b}{8\nu\Upsilon_1 p^{j+\sigma}}\left(\frac{60}{61}\right)^2 \|H_q \tilde{F}^{j+\sigma}\|^2.$$

Hence,

$$w_0\|H_q e^{j+1}\|^2 - \sum_{k=1}^{j}(w_{j-k} - w_{j-k+1})\|H_q e^k\|^2 \le w_j\left[\|H_q e^0\|^2 + \frac{b}{8\nu\Upsilon_1 p^{j+\sigma} w_j}\left(\frac{60}{61}\right)^2 \|H_q \tilde{F}^{j+\sigma}\|^2\right].$$

Thus, using Lemma 2.1.1 and noting that $(j+\sigma)\Delta t = \frac{(j+\sigma)(z(T)-z(0))}{N_t} < (z(T)-z(0))$, we get

$$w_0\|H_q e^{j+1}\|^2 - \sum_{k=1}^{j}(w_{j-k}-w_{j-k+1})\|H_q e^k\|^2 \le w_j\widetilde{\chi}, \tag{66}$$

where

$$\widetilde{\chi} = \|H_q e^0\|^2 + \frac{\Gamma(1-\mu)(z(T)-z(0))^\mu}{\tilde{\epsilon}} \max_{0\le l\le N_t-1}\|H_q\tilde{F}^{l+\sigma}\|^2.$$

Now, we proceed as in Theorem 3.3 and can prove by induction that

$$\|H_q e^{j+1}\|^2 \le \widetilde{\chi}, 0 \le j \le N_t - 1. \tag{67}$$

Further, using Lemma 3.5 in (67) we get (61). □

In view of Equation (8), Lemmas 2.2.2 and 2.2.3, we have

$${}_qR_i^{j+\sigma} = \begin{cases} O(\Delta t^{3-\mu}, \widetilde{\Delta} t^2, h^4), & i = 1, N_x - 1, \\ O(\Delta t^{3-\mu}, \widetilde{\Delta} t^2, h^6), & 2 \le i \le N_x - 2. \end{cases} \tag{68}$$

Now we will prove the main convergence theorem.

Theorem 3.8. *Let $u(x,t) \in C^{8,2}([0,b]\times[0,T])$ be the solution of problem (5)–(7), $u(x, \mathcal{Z}^{-1}(z)) \in C^3[z(T)-z(0)]$ for any fixed x, inverse of z is concave, and $\{U_i^j, 0 \le i \le N_x, 1 \le j \le N_t\}$ be the solution of the discrete problem (33)–(35). Then, the following result holds*

$$\|u_i^{j+1} - U_i^{j+1}\| \le c^* O\left(\Delta t^{3-\mu}, \widetilde{\Delta} t^2, h^{4.5}\right), \tag{69}$$

where $c^* = \sqrt{\frac{\widetilde{m}(z(T)-z(0))^\mu\Gamma(1-\mu)}{\tilde{\epsilon}\Upsilon^2}}$, $\tilde{\epsilon} = \frac{8p^{j+\sigma}}{3b}$, and $\widetilde{m}$ is a postive constant independent of h, Δt, and $\widetilde{\Delta} t$.

Proof. Let $\xi_i^{j+1} = u_i^{j+1} - U_i^{j+1}$. Now subtracting the linear system (33)–(35) from (30)–(32) we get

$$\nu H_q\left[w_0\xi_i^{j+1} - \sum_{k=1}^{j}(w_{j-k}-w_{j-k+1})\xi_i^k - w_j\xi_i^0\right] + q^{j+\sigma}H_q\xi_i^{j+\sigma_j} = p^{j+\sigma}\tilde{\delta}_x^2\xi_i^{j+\sigma_j} + {}_qR_i^{j+\sigma}, 1 \le i \le N_x - 1, \tag{70}$$

$$\xi_i^0 = 0, 1 \le i \le N_x - 1, \tag{71}$$

$$\xi_0^j = 0, \xi_{N_x}^j = 0, 1 \le j \le N_t. \tag{72}$$

Since $\xi_i^{j+1} \in D_h^*$, therefore applying Theorem 3.7 to the error equation (70)–(72) we have

$$\|\xi^{j+1}\|^2 \le \hat{C} \max_{0\le l\le N_t-1}\|{}_qR^{l+\sigma}\|^2, 0 \le j \le N_t - 1, \tag{73}$$

where $\hat{C} = \frac{\Gamma(1-\mu)(z(T)-z(0))^\mu}{\tilde{\epsilon}\Upsilon^2}$ and $\tilde{\epsilon} = \left(\frac{61}{60}\right)^2\frac{4\Upsilon_1 p^{j+\sigma}}{b}$.

Thus, we are left to bound $\|_q R^{l+\sigma}\|^2$ in Equation (73). Using Equation (68), and noting $(N_x - 3)h \le b$, we proceed as follows

$$\begin{aligned}\|_q R^{l+\sigma}\|^2 &= h\sum_{i=1}^{N_x-1}\left(R^{l+\sigma}\right)^2\\ &= 2h\Big(O(\Delta t^{3-\mu}, \widetilde{\Delta} t^2, h^4)\Big)^2 + h(N_x-3)\Big(O(\Delta t^{3-\mu}, \widetilde{\Delta} t^2, h^6)\Big)^2\\ &\le 2\Big(O(\Delta t^{3-\mu}, \widetilde{\Delta} t^2, h^{4.5})\Big)^2 + b\Big(O(\Delta t^{3-\mu}, \widetilde{\Delta} t^2, h^6)\Big)^2\\ &\le \widetilde{m}\Big(O(\Delta t^{3-\mu}, \widetilde{\Delta} t^2, h^{4.5})\Big)^2,\end{aligned}$$

where $\widetilde{m}$ is a positive constant, which is independent of l and h.

Substituting the above result into Equation (73) leads immediately to (69). Thus, the proof is complete. □

4 | NUMERICAL RESULTS

In this segment, we present results for three numerical examples to assess the practical performance of the proposed numerical schemes. If $v(x_i, t_j)$ and $V(x_i, t_j)$ are the exact and approximate solutions of problem (1)–(3), respectively, at (x_i, t_j), then the accuracy of the numerical solution will be measured as follows:

$$L_\infty(h, \Delta t) = \|v - V\|_{L_\infty} = \max_{1\le j\le N_t}\max_{1\le i\le N_x}|v(x_i, t_j) - V(x_i, t_j)|, \tag{74}$$

$$L_2(h, \Delta t) = \|v - V\|_{L_2} = \max_{1\le j\le N_t}\sqrt{h\sum_{i=1}^{N_x-1}(v(x_i, t_j) - V(x_i, t_j))^2}. \tag{75}$$

We evaluate the order of convergence as follows:

$$cov.order = \begin{cases} log_2\left(\frac{L_l(h,\Delta t_1)}{L_l(h,\Delta t_2)}\right), & \text{in time,}\\ log_2\left(\frac{L_l(h_1,\Delta t)}{L_l(h_2,\Delta t)}\right), & \text{in space,}\end{cases} \tag{76}$$

where $l = 2$ or ∞.

Example 4.1. ([22, 24]) Let us consider problem (1)–(3) on the domain $(0, 1) \times (0, 1)$ with the assumption that the function $v(x, t) = \sin(\pi x) + x(x - 1)z(t)^2$ is the exact solution.

We solve this problem taking different $z(t)$, $\omega(t)$, $p(t)$, and $q(t)$ functions and display the results in Tables 1–4. L_2–error $\|v - V\|_{L_2}$ and corresponding spatial orders of convergence for the schemes $CFD_{g-\sigma}$ and $PQS_{g-\sigma}$ are given in Table 1 with scale function $z(t) = e^{2t} - 1$, weight function $\omega(t) = e^t$, $q(t) = 1 - \sin t$, and $p(t) = t$. From this table, we observe that

TABLE 1 (Example 4.1) L_2-error and spatial orders of convergence taking $N_t = 7000$, $z(t) = e^{2t} - 1$, and $\omega(t) = e^t$.

		$CFD_{g-\sigma}$		$PQS_{g-\sigma}$	
μ	N_x	L_2-error	cov.order$_x$	L_2-error	cov.order$_x$
0.2	2^2	4.8023e−04	-	2.2043e−04	-
	2^3	3.3416e−05	3.8451	2.5701e−06	6.4224
	2^4	2.1241e−06	3.9756	3.6534e−08	6.1364
0.5	2^2	4.9622e−04	-	2.2816e−04	-
	2^3	3.4539e−05	3.8447	2.6623e−06	6.4212
	2^4	2.2080e−06	3.9674	5.0752e−08	5.7131
0.8	2^2	5.2026e−04	-	2.3959e−04	-
	2^3	3.6218e−05	3.8444	2.7936e−06	6.4223
	2^4	2.3223e−06	3.9631	6.0568e−08	5.5274

the spatial orders of convergence for $\text{CFD}_{g-\sigma}$ and $\text{PQS}_{g-\sigma}$ schemes are almost 4 and at least 4.5 respectively, which are consistent with our theoretical findings. These are the highest spatial order of convergence in comparison to the existing works for solving generalized fractional reaction–diffusion equation (1)–(3).

Moreover, in Tables 2 and 3, we compare the proposed work with the existing works [22, 24] taking $q(t) = 0$, $p(t) = 1$ and different scale and weight functions. Table 2 shows that the temporal order of convergence of the proposed schemes

TABLE 2 (Example 4.1) Comparison with method in [22] taking $\mu = 0.85$ and $N_x = 1000$.

		[22]		$\text{CFD}_{g-\sigma}$		$\text{PQS}_{g-\sigma}$	
	N_t	L_∞-error	cov.order$_t$	L_∞-error	cov.order$_t$	L_∞-error	cov.order$_t$
$z(t) = t$,	50	2.25e−04	-	2.3953e−05	-	2.3953e−05	-
$\omega(t) = 1$	100	9.72e−05	1.21	5.9883e−06	2.00	5.9883e−06	2.00
	200	3.98e−05	1.29	1.4971e−06	2.00	1.4971e−06	2.00
$z(t) = t$,	50	2.56e−04	-	1.7357e−05	-	1.7357e−05	-
$\omega(t) = e^t$	100	1.12e−04	1.19	4.3385e−06	2.00	4.3385e−06	2.00
	200	4.62e−05	1.28	1.0849e−06	1.99	1.0849e−06	1.99

TABLE 3 (Example 4.1) Comparison with method in [24] taking $z(t) = t^2$, $\omega(t) = 1$, and $N_t = 2000$.

		[24]		$\text{CFD}_{g-\sigma}$		$\text{PQS}_{g-\sigma}$	
μ	N_x	L_2-error	cov.order$_x$	L_2-error	cov.order$_x$	L_2-error	cov.order$_x$
0.2	10	5.2701e−3	-	2.6242e−05	-	1.0994e−06	-
	20	1.3131e−3	2.00	1.6544e−06	3.98	1.6088e−08	6.09
	40	3.2791e−4	2.00	1.0874e−07	3.92	5.7686e−09	1.47
0.5	10	5.4177e−3	-	3.8445e−05	-	1.1328e−06	-
	20	1.3497e−3	2.01	2.4113e−06	3.99	2.2719e−08	5.63
	40	3.3704e−4	2.00	1.5556e−07	3.95	1.2212e−08	0.89
0.8	10	5.6052e−3	-	3.9738e−05	-	1.1729e−06	-
	20	1.3961e−3	2.01	2.4969e−06	3.99	2.6947e−08	5.44
	40	3.4862e−4	2.00	1.6044e−07	3.96	1.6123e−08	0.74

TABLE 4 (Example 4.1) L_2-error and spatial order of convergence taking $z(t) = t^2$, $\omega(t) = 1$, $q(t) = 0$, $p(t) = 1$, and $N_t = 20000$ using $\text{PQS}_{g-\sigma}$ scheme.

	$\mu = 0.2$		$\mu = 0.5$		$\mu = 0.8$	
N_x	L_2-error	cov.order$_x$	L_2-error	cov.order$_x$	L_2-error	cov.order$_x$
10	1.1583e−06	-	1.1856e−06	-	1.2218e−06	-
20	1.0822e−08	6.7420	1.1137e−08	6.7341	1.1512e−08	6.7297
40	1.6282e−10	6.0545	2.2935e−10	5.6016	2.7175e−10	5.4047

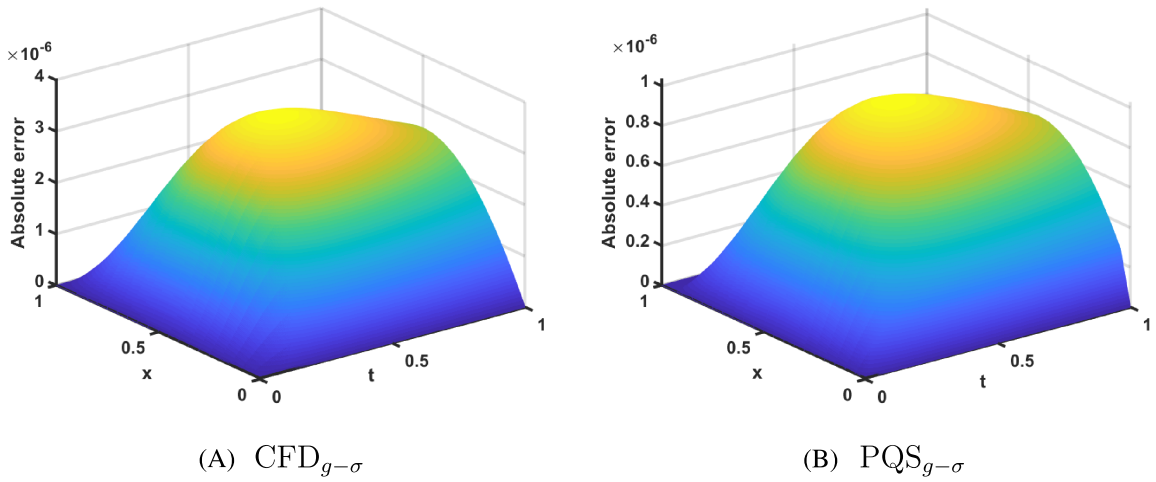

(A) $\text{CFD}_{g-\sigma}$ (B) $\text{PQS}_{g-\sigma}$

FIGURE 1 $L_\infty\left(\frac{1}{20}, \frac{1}{1000}\right)$ with $\mu = 0.8$ for Example 4.1. [Colour figure can be viewed at wileyonlinelibrary.com]

is two, which is higher than the order $2-\mu$ in [22], where μ is the fractional order. Further, from Table 3, it is clear that $\text{CFD}_{g-\sigma}$ and $\text{PQS}_{g-\sigma}$ schemes are more accurate than the scheme in [24]. In this table the order of convergence of $\text{PQS}_{g-\sigma}$ scheme is not as expected, since the temporal mesh width is not sufficiently small. In Table 4, taking $N_t = 20000$, we observe that the convergence order for $\text{PQS}_{g-\sigma}$ scheme is at least 4.5, which is consistent with Theorem 3.8.

Furthermore, Figure 1 represents the absolute error plots for Example 4.1 obtained using $\text{CFD}_{g-\sigma}$ and $\text{PQS}_{g-\sigma}$ schemes taking $z(t) = e^{2t} - 1$, $\omega(t) = e^t$, $p(t) = t$, and $q(t) = 1 - \sin t$. This figure indicates that both proposed schemes approximate the problem well.

Example 4.2. [25] Let us consider problem (5)–(7) on the domain $(0, 1)\times(0, 1)$ with the assumption that the function $u(x, t) = e^x z(t)^\delta$ is the exact solution.

We solve this problem taking $\delta = 3$ and different $p(t)$, $q(t)$, and scale functions $z(t)$ and display the results in Tables 5–8. In Tables 5 and 6, we have taken $p(t) = \sin t$, $q(t) = \cos t$. Further, in Table 5, we have taken $z(t) = \cos(0.1) - \cos(\beta t + 0.1)$ and show that the temporal order of convergence for different fractional order obtained using $\text{CFD}_{g-\sigma}$ scheme is almost 2, which is same as the theoretical order. Similarly, Table 6 displays the temporal order of convergence obtained using

TABLE 5 (Example 4.2) L_2-error and spatial orders of convergence with $h = \frac{1}{500}$ and $z(t) = \cos(0.1) - \cos(\beta t + 0.1)$ using $\text{CFD}_{g-\sigma}$ scheme.

μ	β	N_t	L_2-error	cov. order$_t$	β	L_2-error	cov. order$_t$
0.2	1.1	40	1.9014e−06	-	0.9	7.2140e−07	-
		80	4.9686e−07	1.9362		1.8888e−07	1.9334
		160	1.2761e−07	1.9610		4.8565e−08	1.9594
0.5		40	4.2947e−06	-		1.6137e−06	-
		80	9.8953e−07	2.1177		3.6807e−07	2.1324
		160	2.2997e−07	2.1053		8.4707e−08	2.1194
0.8		40	9.1887e−06	-		3.7050e−06	-
		80	2.1362e−06	2.1048		8.5381e−07	2.1175
		160	4.9573e−07	2.1074		1.9642e−07	2.1200

TABLE 6 (Example 4.2) L_2-error and temporal order of convergence with $h = \frac{1}{500}$ and $z(t) = e^{\beta t} - 1$ using $\text{PQS}_{g-\sigma}$ scheme.

μ	β	N_t	L_2-error	cov. order$_t$	β	L_2-error	cov. order$_t$
0.2	1.1	40	7.5880e−05	-	0.9	2.7976e−05	-
		80	1.9577e−05	1.9546		7.2383e−06	1.9505
		160	4.9885e−06	1.9725		1.8476e−06	1.9700
0.5		40	1.5993e−04	-		6.5261e−05	-
		80	3.8269e−05	2.0632		1.5527e−05	2.0715
		160	9.5408e−06	2.0040		3.7120e−06	2.0645
0.8		40	2.7154e−04	-		1.1513e−04	-
		80	6.5156e−05	2.0592		2.7432e−05	2.0693
		160	1.5623e−05	2.0602		6.5349e−06	2.0696

TABLE 7 (Example 4.2) Comparison with method in [25] taking $z(t) = \cos(0.1) - \cos(\beta t + 0.1)$, $\omega(t) = 1$, $\beta = 1.1$, and $N_t = 20000$.

		[25]		$\text{CFD}_{g-\sigma}$		$\text{PQS}_{g-\sigma}$	
μ	N_x	L_2-error	cov.order$_x$	L_2-error	cov.order$_x$	L_2-error	cov.order$_x$
0.2	5	1.1338e−04	-	2.2775e−07	-	8.5343e−08	-
	10	2.8503e−05	1.9919	1.4241e−08	3.9993	1.4440e−09	5.8851
	20	7.1344e−06	1.9983	8.6531e−10	4.0407	1.2439e−11	6.8590
0.5	5	1.0479e−04	-	2.2775e−07	-	7.9537e−08	-
	10	2.6390e−05	1.9894	1.3163e−08	4.0023	1.3294e−09	5.9028
	20	6.6083e−06	1.9976	7.7203e−10	4.0917	3.5806e−11	5.2144
0.8	5	9.3182e−05	-	1.8815e−07	-	7.1735e−08	-
	10	2.3526e−05	1.9858	1.1728e−08	4.0039	1.2016e−09	5.8997
	20	5.8947e−06	1.9968	6.7337e−10	4.1224	4.7039e−11	4.6749

$PQS_{g-\sigma}$ scheme with $z(t) = e^{\beta t} - 1$. Moreover, for Tables 7 and 8, we have taken $p(t) = 1$, $q(t) = 0$. Table 7 compares the L_2-error and spatial convergence orders obtained using $CFD_{g-\sigma}$ and $PQS_{g-\sigma}$ schemes with the central difference scheme in [25], taking $z(t) = \cos(0.1) - \cos(\beta t + 0.1)$. From this table, we observe that the spatial convergence orders of $CFD_{g-\sigma}$ and $PQS_{g-\sigma}$ scheme are 4 and 4.5, respectively, which are higher than the order 2 in [25]. Furthermore, Table 8 presents a comparison of results identical to those shown in Table 7 but utilizing a different scale function denoted as $z(t) = e^{\beta t} - 1$.

TABLE 8 (Example 4.2) Comparison with method in [25] taking $z(t) = e^{\beta t} - 1$, $\omega(t) = 1$, $\beta = 0.9$, and $N_t = 20000$.

		[25]		$CFD_{g-\sigma}$		$PQS_{g-\sigma}$	
μ	N_x	L_2-error	cov.order$_x$	L_2-error	cov.order$_x$	L_2-error	cov.order$_x$
0.2	5	1.4202e−03	-	2.8513e−06	-	1.0668e−06	-
	10	3.5689e−04	1.9926	1.7824e−07	3.9997	1.7976e−08	5.8911
	20	8.9322e−05	1.9984	1.0787e−08	4.0465	1.7241e−10	6.7041
0.5	5	1.3788e−03	-	2.7702e−06	-	1.0386e−06	-
	10	3.4673e−04	1.9916	1.7278e−07	4.0030	1.7165e−08	5.9190
	20	8.6792e−05	1.9982	1.0057e−08	4.1026	5.4647e−10	4.9732
0.8	5	1.3328e−03	-	2.6803e−06	-	1.0075e−06	-
	10	3.3543e−04	1.9904	1.6696e−07	4.0048	1.6506e−08	5.9316
	20	8.3980e−05	1.9979	9.5043e−09	4.1348	7.5257e−10	4.4550

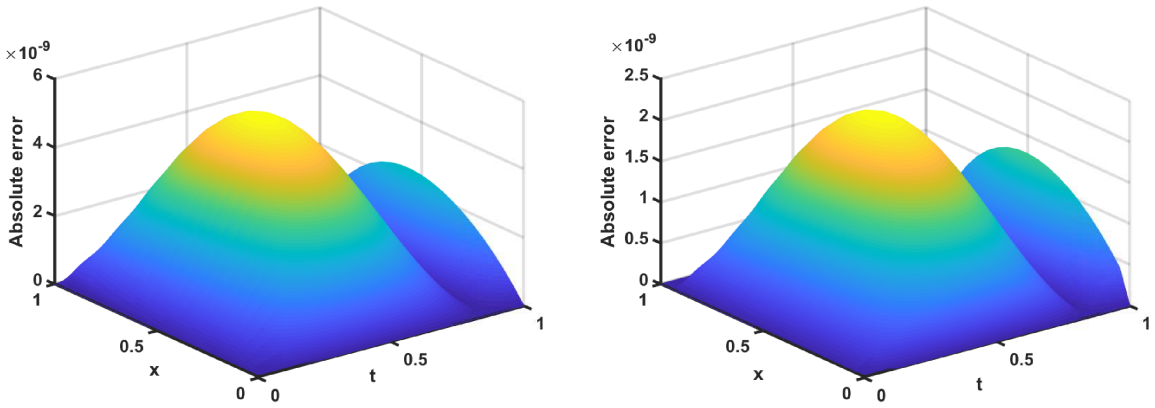

(A) $CFD_{g-\sigma}$ (B) $PQS_{g-\sigma}$

FIGURE 2 $L_\infty\left(\frac{1}{20}, \frac{1}{1000}\right)$ with $\mu = 0.6$ for Example 4.2. [Colour figure can be viewed at wileyonlinelibrary.com]

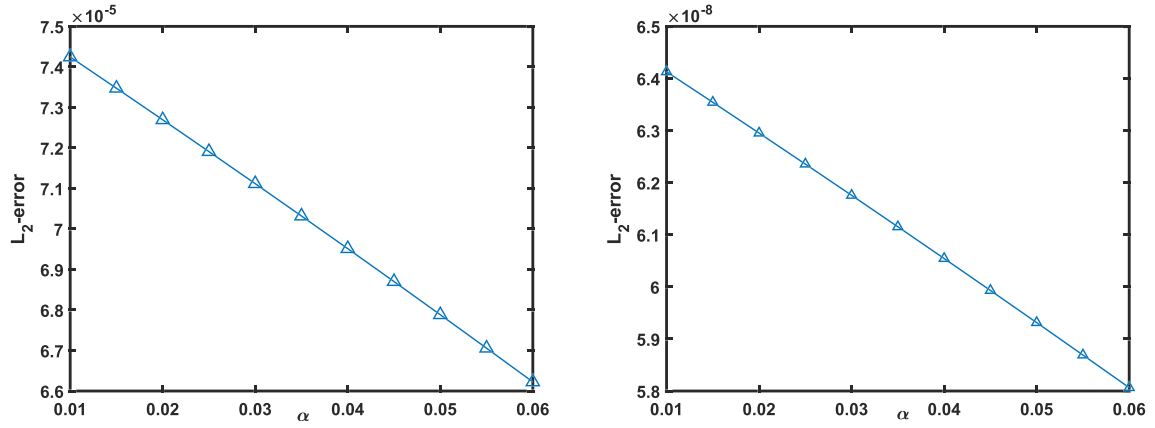

(A) Example 4.1 (B) Example 4.2

FIGURE 3 $L_2\left(\frac{1}{5}, \frac{1}{1000}\right)$ for various α with $\mu = 0.5$. [Colour figure can be viewed at wileyonlinelibrary.com]

Just like Figure 1, we plot the absolute errors in Figure 2 for Example 4.2 obtained using $\text{CFD}_{g-\sigma}$ and $\text{PQS}_{g-\sigma}$ schemes taking $z(t) = \cos(0.1) - \cos(1.1t + 0.1)$, $p(t) = \sin t$, and $q(t) = \cos t$. This figure indicates that we get a good approximation using the proposed schemes. Finally, we examine how alpha affects the errors obtained using $\text{PQS}_{g-\sigma}$ scheme. Therefore, in Figure 3, we plot the L_2-error for different values of $\alpha \in (0, \rho_0)$ and observe that this has little effect on the errors. Hence, α can be chosen to be any value from the interval $(0, \rho_0)$

Example 4.3. [22, 23] Let us consider problem (1)–(3) on the domain $(0, 1) \times (0, 1)$. We will solve this problem taking $\hat{\phi}_1(t) = \hat{\phi}_2(t) = 0$, $g_0(x) = x(1-x)^3 e^{\sin 3.5\pi x}$, $q(t) = 0$, and source function $\mathcal{F}(x, t) = \frac{(x-1)(t-1)}{2+\sin xt}$.

In this problem, we will provide a few plots to examine the effect of the scale function $z(t)$, the weight function $\omega(t)$, and the diffusion function $p(t)$ on the solution obtained using $\text{CFD}_{g-\sigma}$ scheme. So, we have fixed the values $\mu = 0.92$, $N_x = 150$, and $N_t = 1000$ to make a fair comparison in all the cases.

In Figure 4, we plot the three-dimensional graphics of the discrete solution under the four cases given below:

1. $\omega(t) = e^t$, $z(t) = t$, and $p(t) = 1.2$; (base case).
2. $\omega(t) = e^t$, $z(t) = t^6$, and $p(t) = 1.2$; (change $z(t)$).
3. $\omega(t) = e^{6t}$, $z(t) = t$, and $p(t) = 1.2$; (change $\omega(t)$).
4. $\omega(t) = e^t$, $z(t) = t$, and $p(t) = 0.6$; (change $p(t)$).

The following are the observations

- From Figure 4A, we can observe that the numerical solution eventually tends to zero, as we have used zero boundary conditions.

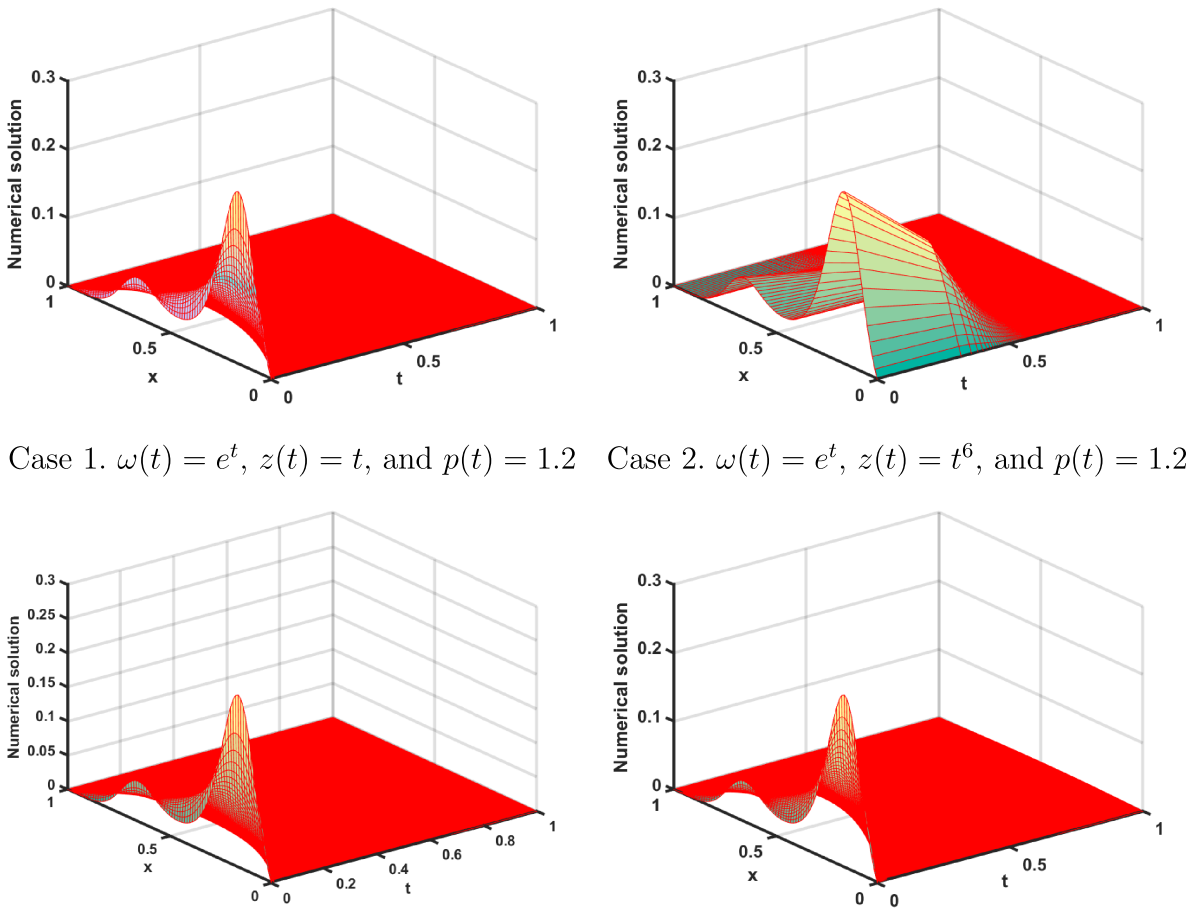

FIGURE 4 Numerical solutions of Example 4.3. [Colour figure can be viewed at wileyonlinelibrary.com]

- From Figure 4B, we see that as the scale function is contracted, the stretching of the time domain takes place near $t = 0$, which provides a coarser mesh compared to Figure 4A.
- In Figure 4C, we have taken a larger weight function $\omega(t) = e^{6t}$ as compared to Figure 4A, which shows the solution has become smaller. Furthermore, we can observe from this figure that the diffusion phenomenon is fast due to the monotonically increasing weight function.
- In Figure 4D, we have assumed a smaller value of diffusion function ($p(t) = 0.6$) than in Figure 4A ($p(t) = 1.2$); consequently, the diffusion process slows down in this case.

5 | CONCLUSION

In this work, two high-order schemes, $\text{CFD}_{g-\sigma}$ and $\text{PQS}_{g-\sigma}$, have been developed for numerically solving a variable coefficients generalized fractional reaction–diffusion equation. The $\text{CFD}_{g-\sigma}$ scheme combined the $gL2{-}1_\sigma$ approximation of fractional time derivative with a compact space difference scheme, whereas the $\text{PQS}_{g-\sigma}$ scheme has been formulated using the $gL2 - 1_\sigma$ formula for the temporal discretization along with the parametric quintic splines for the spatial discretization. The theoretical analysis, which included the stability and convergence of both schemes, has been rigorously established using the discrete energy method in L_2-norm. The convergence orders $O(\Delta t^{3-\mu}, \widetilde{\Delta} t^2, h^4)$ and $O(\Delta t^{3-\mu}, \widetilde{\Delta} t^2, h^{4.5})$ of $\text{CFD}_{g-\sigma}$ and $\text{PQS}_{g-\sigma}$ schemes, respectively, have improved the existing works and are best till date for variable coefficients generalized fractional reaction–diffusion equations. Finally, numerical experiments have been performed to show the accuracy and efficiency of the proposed schemes. Our intention for the future is to expand the current approach to encompass non-linear generalized fractional problems, as well as to higher dimensional generalized fractional problems.

ACKNOWLEDGEMENTS

The first author gratefully acknowledge the support of University Grant Commission, India, for research fellowship. The authors gratefully acknowledge the valuable comments and suggestions from the anonymous referees.

CONFLICT OF INTEREST STATEMENT

The authors have no relevant financial or nonfinancial interests to disclose.

DATA AVAILABILITY STATEMENT

Data availability is not applicable for this paper.

ORCID

Anshima Singh https://orcid.org/0000-0001-6317-3011
Jesus Vigo-Aguiar https://orcid.org/0000-0002-1921-6579

REFERENCES

1. A. A. Kilbas, H. M. Srivastava, and J. J. Trujillo, *Theory and applications of fractional differential equations*, Vol. **204**, elsevier, 2006.
2. K. S. Miller and B. Ross, *An introduction to the fractional calculus and fractional differential equations*, Wiley, 1993.
3. F. Mainardi and A. Carpinteri, *Fractals and fractional calculus in continuum mechanics*, Springer, 1997.
4. A. Singh and S. Kumar, *A convergent exponential B-spline collocation method for a time-fractional telegraph equation*, Comput. Appl. Math. **42** (2023), no. 2, 79.
5. J. A. T. M. J. Sabatier, O. P. Agrawal, and JAT Machado, *Advances in fractional calculus: Theoretical developments and applications in physics and engineering*, Vol. **4**, Springer, 2007.
6. C. Ionescu, A. Lopes, D. Copot, JAT Machado, and J. H. T. Bates, *The role of fractional calculus in modeling biological phenomena: A review*, Commun. Nonlinear Sci. Numer. Simul. **51** (2017), 141–159.
7. A. S. El-Karamany and M. A. Ezzat, *On fractional thermoelasticity*, Math. Mech. Solids **16** (2011), no. 3, 334–346.
8. Y. Povstenko, *Linear fractional diffusion-wave equation for scientists and engineers*, Springer, 2015.
9. S.-B. Chen, H. Jahanshahi, O. A. Abba, J. E. Solís-Pérez, S. Bekiros, J. F. Gómez-Aguilar, A. Yousefpour, and Y.-M. Chu, *The effect of market confidence on a financial system from the perspective of fractional calculus: Numerical investigation and circuit realization*, Chaos, Solitons Fract. **140** (2020), 110223.

10. P. Veeresha, D. G. Prakasha, and S. Kumar, *A fractional model for propagation of classical optical solitons by using nonsingular derivative*, 2020. Mathematical Methods in the Applied Sciences.
11. S. Kumar, R. Kumar, C. Cattani, and B. Samet, *Chaotic behaviour of fractional predator-prey dynamical system*, Chaos, Solitons Fract. **135** (2020), 109811.
12. D. Baleanu, M. Jleli, S. Kumar, and B. Samet, *A fractional derivative with two singular kernels and application to a heat conduction problem*, Adv. Differ. Equ. **2020** (2020), 1–19.
13. D. Baleanu, A. Jajarmi, H. Mohammadi, and S. Rezapour, *A new study on the mathematical modelling of human liver with Caputo–Fabrizio fractional derivative*, Chaos, Solitons Fract. **134** (2020), 109705.
14. K. Khari and V. Kumar, *An efficient numerical technique for solving nonlinear singularly perturbed reaction diffusion problem*, J. Mathe. Chem. **60** (2022), no. 7, 1356–1382.
15. J. Crank, *The mathematics of diffusion*, Oxford university press, 1979.
16. J. De Wilde and G. F. Froment, *Computational fluid dynamics in chemical reactor analysis and design: Application to the ZoneFlow reactor for methane steam reforming*, Fuel **100** (2012), 48–56.
17. H. Y. Alfifi, *Stability and Hopf bifurcation analysis for the diffusive delay logistic population model with spatially heterogeneous environment*, Appl. Math. Comput. **408** (2021), 126362.
18. K. Seki, M. Wojcik, and M. Tachiya, *Fractional reaction-diffusion equation*, The J. Chem. Phys. **119** (2003), no. 4, 2165–2170.
19. A. Jajarmi, D. Baleanu, S. S. Sajjadi, and J. J. Nieto, *Analysis and some applications of a regularized Ψ-Hilfer fractional derivative*, J. Comput. Appl. Math. **415** (2022), 114476.
20. O. P. Agrawal, *Some generalized fractional calculus operators and their applications in integral equations*, Fract. Calc. Appl. Anal. **15** (2012), no. 4, 700–711.
21. M.-H. Kim, G.-C. Ri, and O. Hyong-Chol, *Operational method for solving multi-term fractional differential equations with the generalized fractional derivatives*, Fract. Calc. Appl. Anal. **17** (2014), no. 1, 79–95.
22. Y. Xu, Z. He, and O. P. Agrawal, *Numerical and analytical solutions of new generalized fractional diffusion equation*, Comput. Math. Appl. **66** (2013), no. 10, 2019–2029.
23. X. Li and P. J. Y. Wong, *A gWSGL numerical scheme for generalized fractional sub-diffusion problems*, Commun. Nonlinear Sci. Numer. Simul. **82** (2020), 104991.
24. X. Li and P. J. Y. Wong, *Gl 1 scheme for solving a class of generalized time-fractional diffusion equations*, Mathematics **10** (2022), no. 8, 1219.
25. X. Li and P. J. Y. Wong, *Generalized Alikhanov's approximation and numerical treatment of generalized fractional sub-diffusion equations*, Commun. Nonlinear Sci. Numer. Simul. **97** (2021), 105719.
26. Y. Xu and O. P. Agrawal, *Numerical solutions and analysis of diffusion for new generalized fractional Burgers equation*, Fract. Calc. Appl. Anal. **16** (2013), no. 3, 709–736.
27. Y. Xu, Z. He, and Q. Xu, *Numerical solutions of fractional advection–diffusion equations with a kind of new generalized fractional derivative*, Int. J. Comput. Math. **91** (2014), no. 3, 588–600.
28. M. A. Dablain, *The application of high-order differencing to the scalar wave equation*, Geophysics **51** (1986), no. 1, 54–66.
29. H.-L. Liao, Z.-Z. Sun, and H.-S. Shi, *Error estimate of fourth-order compact scheme for linear Schrödinger equations*, SIAM J. Numer. Anal. **47** (2010), no. 6, 4381–4401.
30. M. Cui, *Compact finite difference method for the fractional diffusion equation*, J. Comput. Phys. **228** (2009), no. 20, 7792–7804.
31. G. Gao and Z. Sun, *A compact finite difference scheme for the fractional sub-diffusion equations*, J. Comput. Phys. **230** (2011), no. 3, 586–595.
32. M. Ran and C. Zhang, *New compact difference scheme for solving the fourth-order time fractional sub-diffusion equation of the distributed order*, Appl. Numer. Math. **129** (2018), 58–70.
33. S. Sumit, S. Kumar, and M. Kumar, *Optimal fourth-order parameter-uniform convergence of a non-monotone scheme on equidistributed meshes for singularly perturbed reaction–diffusion problems*, Int. J. Comput. Math. **99** (2022), no. 8, 1638–1653.
34. L. L. Ferrás, N. Ford, M. L. Morgado, and M. Rebelo, *High-order methods for systems of fractional ordinary differential equations and their application to time-fractional diffusion equations*, Math. Comput. Sci. **15** (2021), no. 4, 535–551.
35. S. Kumar and J. Vigo-Aguiar, *A high order convergent numerical method for singularly perturbed time dependent problems using mesh equidistribution*, Math. Comput. Simul. **199** (2022), 287–306.
36. S. C. S. Rao and S. Kumar, *Robust high order convergence of an overlapping Schwarz method for singularly perturbed semilinear reaction-diffusion problems*, J. Comput. Math. **2013** (2013), 509–521.
37. S. C. S. Rao and S. Kumar, *An almost fourth order uniformly convergent domain decomposition method for a coupled system of singularly perturbed reaction–diffusion equations*, J. Comput. Appl. Math. **235** (2011), no. 11, 3342–3354.
38. V. Gupta, M. Kumar, and S. Kumar, *Higher order numerical approximation for time dependent singularly perturbed differential-difference convection-diffusion equations*, Numer. Methods Partial Differ. Equ. **34** (2018), no. 1, 357–380.
39. S. Kumar and M. Kumar, *High order parameter-uniform discretization for singularly perturbed parabolic partial differential equations with time delay*, Comput. Math. Appl. **68** (2014), no. 10, 1355–1367.
40. S. Jator and Z. Sinkala, *A high order B-spline collocation method for linear boundary value problems*, Appl. Math. Comput. **191** (2007), no. 1, 100–116.
41. R. C. Mittal and G. Arora, *Quintic B-spline collocation method for numerical solution of the Kuramoto–Sivashinsky equation*, Commun. Nonlinear Sci. Numer. Simul. **15** (2010), no. 10, 2798–2808.

42. F.-G. Lang and X.-P. Xu, *Quintic B-spline collocation method for second order mixed boundary value problem*, Comput. Phys. Commun. **183** (2012), no. 4, 913–921.
43. A. Khan, M. A. Noor, and T. Aziz, *Parametric quintic-spline approach to the solution of a system of fourth-order boundary-value problems*, J. optim. Theory Appl. **122** (2004), no. 2, 309–322.
44. S. M. Hosseini and R. Ghaffari, *Polynomial and nonpolynomial spline methods for fractional sub-diffusion equations*, Appl. Math. Model. **38** (2014), no. 14, 3554–3566.
45. T. S. El-Danaf and A. R. Hadhoud, *Parametric spline functions for the solution of the one time fractional Burgers equation*, Appl. Math. Model. **36** (2012), no. 10, 4557–4564.
46. X. Li and P. J. Y. Wong, *A higher order non-polynomial spline method for fractional sub-diffusion problems*, J. Comput. Phys. **328** (2017), 46–65.
47. A. Khan and T. Sultana, *Parametric quintic spline solution for sixth order two point boundary value problems*, Filomat **26** (2012), no. 6, 1233–1245.
48. A. Khan and T. Sultana, *Parametric quintic spline solution of third-order boundary value problems*, Int. J. Comput. Math. **89** (2012), no. 12, 1663–1677.
49. X. Li and P. J. Y. Wong, *Non-polynomial spline approach in two-dimensional fractional sub-diffusion problems*, Appl. Math. Comput. **357** (2019), 222–242.

How to cite this article: A. Singh, S. Kumar, and J. Vigo-Aguiar, *High-order schemes and their error analysis for generalized variable coefficients fractional reaction–diffusion equations*, Math. Meth. Appl. Sci. **46** (2023), 16521–16541, DOI 10.1002/mma.9458.